AGU PUBLICATIONS

Geophysical Research Letters

RESEARCH LETTER
10.1002/2017GL075814

Key Points:
- Responses of Jupiter's northern aurora spectra to Io volcanic activity were detected using Hisaki/EXCEED long-term monitoring
- Decrease of color ratio, that is, auroral electron energy, suggests reduced electron acceleration for the more highly populated magnetosphere
- Long-term observation provided the typical value and variances of auroral emission power and electron parameters

Supporting Information:
- Supporting Information S1

Correspondence to:
C. Tao,
chihiro.tao@nict.go.jp

Citation:
Tao, C., Kimura, T., Tsuchiya, F., Muirakami, G., Yoshioka, K., Yamazaki, A., … Fujimoto, M. (2018). Variation of Jupiter's aurora observed by Hisaki/EXCEED: 3. Volcanic control of Jupiter's aurora. *Geophysical Research Letters*, *45*, 71–79. https://doi.org/10.1002/2017GL075814

Received 24 SEP 2017
Accepted 12 DEC 2017
Accepted article online 29 DEC 2017
Published online 10 JAN 2018

Variation of Jupiter's Aurora Observed by Hisaki/EXCEED: 3. Volcanic Control of Jupiter's Aurora

Chihiro Tao[1,2], Tomoki Kimura[3], Fuminori Tsuchiya[4], Go Muirakami[5], Kazuo Yoshioka[6], Atsushi Yamazaki[5], Sarah V. Badman[7], Hiroaki Misawa[4], Hajime Kita[2], Yasumasa Kasaba[2], Ichiro Yoshikawa[6], and Masaki Fujimoto[5]

[1]National Institute of Information and Communications Technology, Koganei, Japan, [2]Department of Geophysics, Tohoku University, Sendai, Japan, [3]RIKEN, Saitama, Japan, [4]Planetary Plasma and Atmospheric Research Center, Graduate School of Science, Tohoku University, Sendai, Japan, [5]ISAS/JAXA, Sagamihara, Japan, [6]Department of Complexity Science and Engineering, University of Tokyo, Kashiwa, Japan, [7]Physics Department, Lancaster University, Lancaster, UK

Abstract Temporal variation of Jupiter's northern aurora during enhanced Io volcanic activity was detected using the EXCEED spectrometer on board the Hisaki Earth-orbiting planetary space telescope. It was found that in association with reported Io volcanic events in early 2015, auroral power and estimated field-aligned currents were enhanced during day of year 40–120. Furthermore, the far ultraviolet color ratio decreased during the event, indicating a decrease of auroral electron mean energy and total acceleration by $<$30%. During the episode of enhanced Io volcanic activity, Jupiter's magnetosphere contains more source current via increased suprathermal plasma density by up to 42%; therefore, it would have required correspondingly less electron acceleration to maintain the enhanced field-aligned current and corotation enforcement current. Sporadic large enhancements in auroral emission detected more frequently during the active period could have been contributed by nonadiabatic magnetospheric energization.

1. Introduction

The Jovian magnetosphere is characterized by a plasma supply of up to ~1 t s^{-1} from its volcanically active moon, Io. Despite the initial radial transport of the plasma, its rotational motion around Jupiter is maintained by the transfer of angular momentum from the planetary atmosphere (e.g., Hill, 1979). Jupiter's main aurora is considered to be produced by the angular momentum transfer carried by the field-aligned current (e.g., Cowley & Bunce, 2001; Hill, 2001).

The level of volcanic activity of Io can change dramatically; the subsequent enhancement in the emission of the Io plasma torus (IPT) can persist for a few days to a period of several months. In association with the volcanic activation in May 2007 detected via brightening of the sodium nebula observation by Yoneda, Kagitani, and Okano (2009), an auroral image after the enhancement showed an equatorward shift of the main aurora and an increase in the occurrence of very bright enhancement $>$600 GW at lower latitudes (Bonfond et al., 2011). On the other hand, the activity of aurora-related hectometric radio emission was reduced (Yoneda et al., 2013). As momentum transfer is supposed to occur efficiently over a more limited radial distance of the equatorial magnetosphere for the increased plasma case, theoretical models predict that the main aurora would be located at lower latitudes for the case of increased Io plasma mass loading (Nichols, 2011; Nichols & Cowley, 2005; Tao, Fujiwara, & Kasaba, 2010). Nichols (2011) suggested that the field-aligned current, that is, intensity of the main auroral emission, would increase or decrease when variation in plasma production occurs with or without the modification of the background plasma density, respectively. In order to associate these different features of the aurora (i.e., auroral intensity and particle acceleration) with the resultant auroral electron energy, continuous auroral spectral observation is required.

This monitoring can be achieved by JAXA's Hisaki Earth-orbiting space telescope. The EXCEED (Extreme Ultraviolet Spectroscope for Exospheric Dynamics) spectrometer on board Hisaki monitors emissions from both the IPT and Jupiter's northern aurora simultaneously (Yamazaki et al., 2014; Yoshikawa et al., 2014; Yoshioka et al., 2013). Ground-based monitoring of the sodium line from Jupiter magnetosphere showed enhancement and radial extension on the eastern side starting from 10 January 2015 (day of year (DOY) 10) (Yoneda et al., 2015). Infrared imaging of Io's surface detected a sudden brightness enhancement at

Kurdalagon Patera on 26 January (de Kleer & de Pater, 2016). The intensity of emission from the sodium neutral cloud subsequently increased by almost a factor of 4 by the middle of February before decreasing in April. This emission enhancement is actually weak compared to typical events (Yoneda et al., 2015). This variation in neutral sodium emission was followed by enhancements of IPT S^+ (increase from DOY 20 and decrease during DOY ~60–90), S^{2+} (increase from DOY ~30 and decrease during DOY 70–110), and S^{3+} lines (increase from DOY ~40 and decrease from DOY 90) detected by EXCEED (Tsuchiya et al., 2017MOP, Yoshikawa et al., 2017). EXCEED cannot resolve auroral structure due to its moderate spatial resolution (~1 R_J around Jupiter's opposition), but it can monitor auroral spectra continuously for ~40 min during each 106 min orbit. Applying the spectral analysis proposed by Tao, Kimura, Badman, Murakami, et al., (2016) and Tao, Kimura, Badman, André, et al., (2016) (hereafter Paper I and Paper II, respectively), the auroral and magnetospheric responses to the described volcanic activity are investigated in this study.

2. Observations and Data Procedure

The Hisaki auroral observations and analysis are described in detail for the reader by Kimura et al. (2015), Paper I, and Paper II; therefore, we only describe them briefly herein. The northern auroral region is covered by the dawn-dusk directed dumbbell-shaped slit with an effective spatial resolution of 17 arcsec and a pointing accuracy of ±2 arcsec. EXCEED detects auroral emissions over the 80–148 nm wavelength range, covering part of the H_2 Lyman and Werner band emissions with full width at half maximum (FWHM) resolution of 0.3 nm. The auroral signals within the 20 arcsec aperture of the slit width are integrated for each specific wavelength. The waveband 138.5–144.8 nm is used to estimate the total emission and input power. The far ultraviolet color ratio (CR) is defined as the ratio of the intensity of the waveband absorbed least by atmospheric hydrocarbons (138.5–144.8 nm) to that absorbed most (123–130 nm), which for EXCEED is defined as CR_{EXCEED}. As the CR reflects the depth of the auroral electron precipitation into the hydrocarbon layer, the auroral electron energy can be estimated assuming a particular atmosphere model. The total number flux derived from the electron energy and energy flux is converted into the field-aligned current density, using an averaged auroral area based on an empirical magnetic field model called VIP4 (Connerney et al., 1998). With reference to the auroral electron acceleration theory, the source current density can then be estimated (Paper II). We analyzed observations when the Jupiter northern aurora was facing Earth, that is, when the central meridional longitude (CML) was 45–345° system III longitude. As the auroral oval around the northern pole is shifted from Jupiter's rotational pole, the auroral aperture and thus the auroral power detectable from Earth varies with Jupiter's rotation. This aperture effect on the total power is scaled by multiplying by the factor, (maximum visible auroral length integrated over all CML)/(visible auroral length at instantaneous CML), assuming a typical auroral location (Paper II), which is called "revised power" hereafter.

The solar wind conditions just upstream of Jupiter's magnetosphere are estimated using a one-dimensional magnetohydrodynamic model that propagates the solar wind variation observed at Earth toward Jupiter (Tao et al., 2005). Here we used OMNI 1 h data as the input for this propagation model.

3. Results

Figure 1 shows an overview of the variation of the auroral parameters (Figures 1a–1c) and the IPT power (Figure 1d) for two periods: season 2014 (December 2013 to April 2014) and season 2015 (November 2014 to May 2015). Auroral intensity enhancements can be observed in minimum-hydrocarbon absorption wavebands within the Hisaki/EXCEED wavelength range (Figure 1a) and the total emitted power (Figure 1b). These are associated with the enhancement of the source current density $j_{//0}(2.5/k_B T_0$ [keV]) before the field-aligned acceleration of the magnetospheric electrons occurs (Figure 1c). Several enhancements over a few days during the observation periods are related to enhancements due to the solar wind dynamic pressure (Figure 1e), whereas the aurora shows a characteristic variation associated with the long-term IPT enhancement (Figure 1d). All estimated parameters are provided in the supporting information (Figure S1).

Compared with season 2014 and the early part of season 2015 (until DOY 40), the aurora shows larger enhancements more frequently after DOY 40 in 2015. With reference to the more continuous observations in season 2015, auroral enhancements beyond 50 GW in the 136.5–144.8 nm waveband can be seen on DOY −33 to −32, −7, 12–14, 41, 48–49, 66, 70, 72, 74, 87, 96, 103, 116, and 127 in 2015 (Figure 1a), that is, 3 events in the first 80 days (DOY −40 to 40) and 11 events in the second 80 days (DOY 40–120).

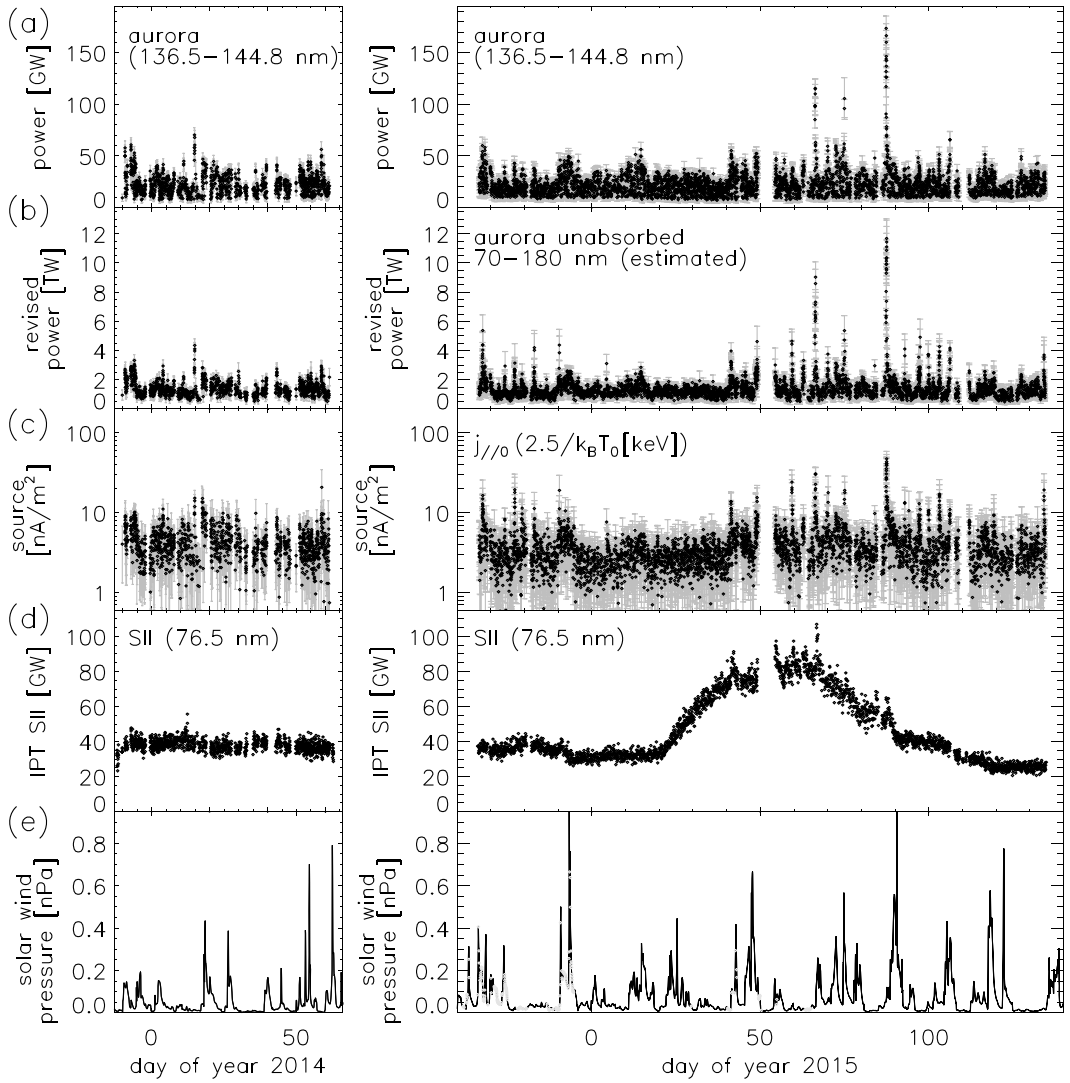

Figure 1. Time variations of the auroral powers emitted at wavelength (a) 138.5–144.8 nm, (b) appearance normalized total unabsorbed H_2 power over wavelength 70–180 nm, (c) maximum field-aligned current that can be carried by precipitating magnetospheric electrons without field-aligned acceleration, shown for the electron temperature k_BT_0 = 2.5 keV case, (d) IPT SII emission (see Yoshikawa et al., 2017 for detail), and (e) solar wind dynamic pressure for season 2014 (left column) and season 2015 (right column). Grey vertical lines in Figures 1a–1c show errors estimated based on the photon statistics. Solar wind input data in season 2015 are not complete, which would affect the output grey points in Figure 1e.

Among them, very large enhancements of the power in the 136.5–144.8 nm waveband reach 115, 105, and 173 GW on DOY 66, 74, and 87 in 2015, respectively. As the emission intensity of maximum-hydrocarbon absorption waveband (126.3–130.0 nm) also increases (Figure S1b), the CRs and electron energies for these events are not large; their medians and standard deviations (1σ) of the electron energy are 165 ± 38, 165 ± 23, and 159 ± 31 keV, respectively, slightly smaller than the value of 178 ± 39 keV derived from the entire data set within a statistically insignificant level (0.33σ–0.49σ, where σ = 39 keV). On the other hand, their electron fluxes reach 282, 268, and 431 MA, which are 5.2, 5.0, and 7.9 times larger than the mean value over the entire period, respectively.

Figure 2a shows the CR_{EXCEED} as a function of CML comparing before (DOY 0–30, blue) and after (50–80, red) the volcanic activity enhancement. CR_{EXCEED} at CML 175–225° decreases significantly during the active period by up to 30%. We divided the data into two groups: auroral power enhancement events (EV, red points in Figures 2b–2d) whose revised auroral power at 136.5–144.8 nm reaches >45 GW and other backgrounds

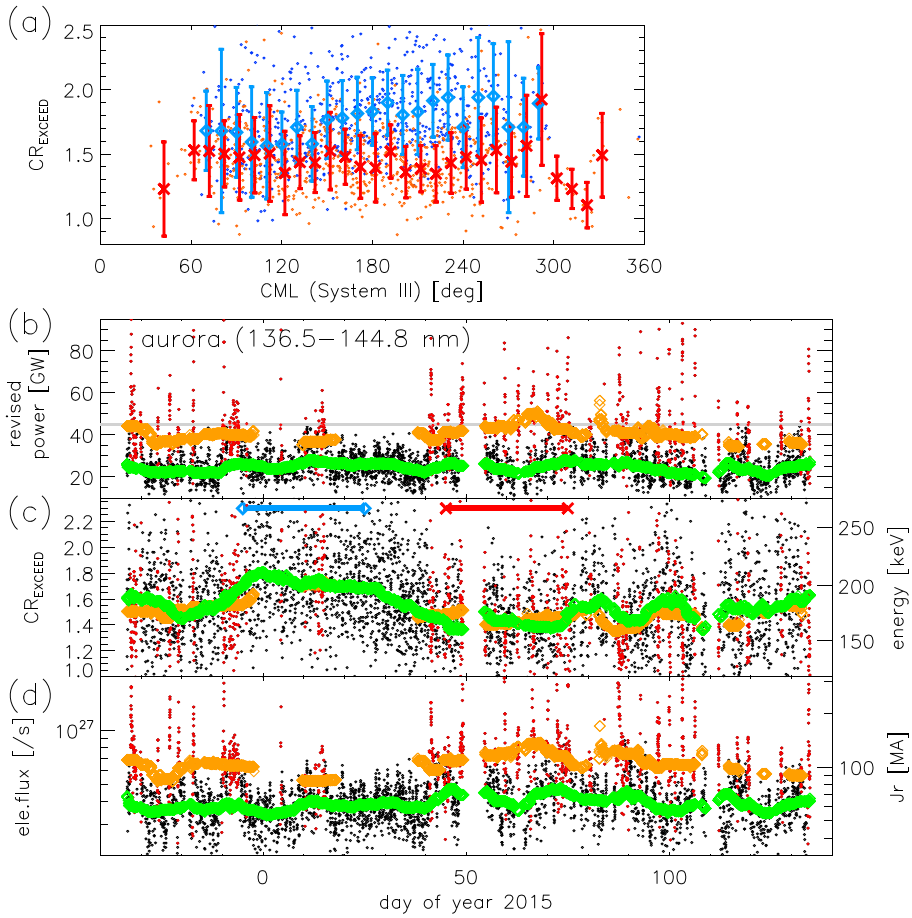

Figure 2. (a) CR_{EXCEED} as a function of CML in system III and time variations of (b) the power emitted at the wavelength 138.5–144.8 nm, (c) CR_{EXCEED} and (d) auroral electron flux for season 2015. Blue (red) points in Figure 2a are observed on DOY −5–25 (45–75) in 2015, and diamonds (crosses) are mean values over 10° binned CML with error bars showing variances. In Figures 2b–2d, the enhancement event (EV) and backgrounds (BG) are shown by red and black points, respectively, and 10 day running average of EV and BG are shown by orange and green marks, respectively. The 45 GW threshold is shown by grey line in Figure 2b. Corresponding auroral electron energy and total current are shown on the right-hand *y* axes of Figures 2b and 2c, respectively.

(BG, black points). As discussed above, the occurrences of these events vary. Ten day running averages of both EV and BG show a decrease in CR_{EXCEED} after DOY ~40 in 2015 (Figure 2c), and a slight increase in electron flux (Figure 2d) with almost constant power (Figure 2b) is seen for BG.

Table 1 lists the median values of the key parameters over five selected periods: (i) season 2014, (ii) DOY −40 to 40, (iii) DOY 40 to 120, (iv) DOY 120 to 140 of season 2015, and (v) the entire data set. The error values represent the standard deviation. The standard deviation of the emission power, electron flux, and source current density increase during the period of Io-enhanced activity; for example, the standard deviation of the revised total emission power is 1,175 GW in (iii) and 493–512 GW in the other periods.

Figure 3a shows the relationship between the mean electron energy and energy flux taken from the active (period (iii), orange points) and other quiet periods (periods (ii) and (iv), black points) in season 2015. For the active period, the mean energy decreases as seen in Figure 2c and energy flux mainly increases with a broadening of its distribution. The difference between the two distributions is evident in the contour maps of each period shown in Figures 3b and 3c. We derived best-fit Knight relation curves with a density of source 2.5 keV electrons that minimizes the root-mean-square error (RMSE) of the data. We used 90% of the data points, which have energy flux and mean energy values closest to the average of each value. Moreover, the density becomes 0.0019 and 0.0027 cm^{-3} during the quiet and active periods, respectively. The

Table 1
Medians and Standard Deviations of Key Parameters During Each Period

	(i) 19 Dec 2013 to 3 Mar 2014 season 2014	(ii) 27 Nov 2014 to 9 Feb 2015 DOY −40 to 40	(iii) 9 Feb 2015 to 18 May 2015 DOY 40 to 120	(iv) 23 Feb 2015 to 14 May 2015 DOY 120 to 140	(v) All
Power 138.5–144.8 nm (GW)	21.2 ± 9.69	19.7 ± 8.36	21.8 ± 15.1	18.9 ± 6.94	20.7 ± 11.4
Power 126.3–130.0 nm (GW)	16.4 ± 7.47	13.6 ± 5.71	16.2 ± 11.2	13.5 ± 4.48	15.1 ± 8.45
CR_{EXCEED}	1.42 ± 0.37	1.62 ± 0.36	1.46 ± 0.31	1.54 ± 0.33	1.51 ± 0.35
Electron energy (keV)	167. ± 37.	191. ± 41.	171. ± 35.	181. ± 38.	178. ± 39.
Total power (GW)	984. ± 449.	915. ± 389.	1009. ± 701.	871. ± 324.	962. ± 529.
Electron flux (MA)	58.5 ± 26.4	48.9 ± 20.3	58.0 ± 40.1	48.2 ± 15.9	54.2 ± 30.0
Electron flux ($\mu A\ m^{-2}$)	0.267 ± 0.106	0.216 ± 0.109	0.266 ± 0.254	0.210 ± 0.110	0.243 ± 0.175
$j_{//0}(2.5/k_BT_0$ (keV)) ($nA\ m^{-2}$)	4.01 ± 2.08	2.88 ± 2.02	3.94 ± 4.22	2.96 ± 2.05	3.42 ± 3.03
Solar wind pressure (nPa)	0.025 ± 0.070	0.037 ± 0.073	0.049 ± 0.117	0.021 ± 0.090	0.032 ± 0.082
System III longitude (deg)	173. ± 61.	176. ± 60.	173. ± 63.	172. ± 54.	174. ± 60.
Revised total power (GW)	1,311. ± 493.	1,214. ± 509.	1,363. ± 1175.	1,124. ± 512.	1,276. ± 810.

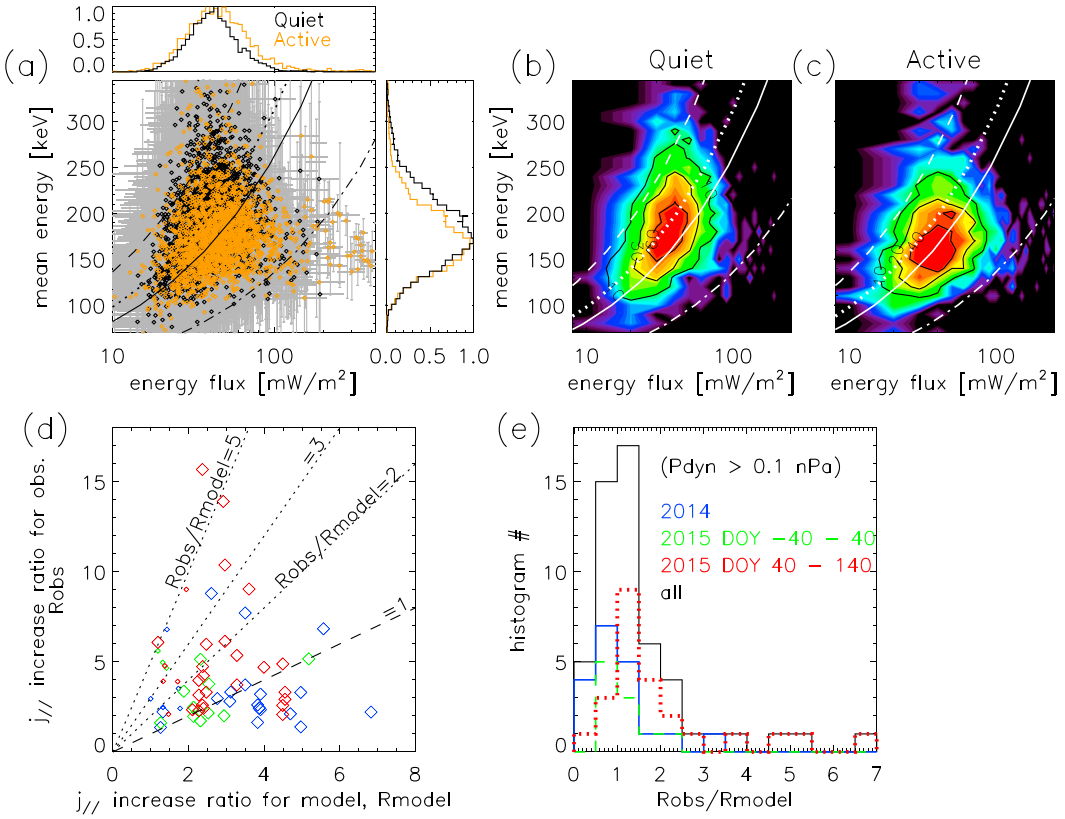

Figure 3. Relationship between the mean energy and energy flux of the precipitating auroral electrons estimated from 10 min integrated observations shown as (a) a scatter plot using data during the quiet (black dots) and active (orange dots) volcanic periods in season 2015, and occurrence map for the (b) quiet and (c) active volcanic periods separately. Grey lines in Figure 3a are error bars, and mean energy and energy flux distributions are plotted as histograms normalized by maximum occurrence values in the right and upper panels, respectively, for each period separately. The Knight relation is shown for different source populations: $N_0 = 0.0027\ cm^{-3}$ (solid lines), $N_0 = 0.0019\ cm^{-3}$ (dotted lines), $N_0 = 0.001\ cm^{-3}$ (dashed lines), and $N_0 = 0.01\ cm^{-3}$ (dash-dotted lines) (e.g., Gustin et al., 2004). (d) Increase ratio of the estimated field-aligned current (see text in detail) R_{model}, compared with the value derived from the observation, R_{obs}, and (e) histogram of R_{obs}/R_{model} whose solar wind pressure >0.1 nPa. Color indicates different periods: 2014 seasons (blue), before the Io volcanic active in 2015 (green), and during the active time (red), and their sum (black in Figure 3e). Large diamonds in Figure 3d show the cases whose dynamic pressure reach >0.1 nPa, dashed line shows $R_{obs}/R_{model} = 1$, and dotted lines show $R_{obs}/R_{model} = 2$, 3, and 5.

goodness of fit is confirmed by a good distributional correlation between the concentrations of data shown in red (27% occurrence), with the white curves representing the best-fit Knight relation curves. The derived minimum RMSEs for these two periods are relatively small such that their difference is statistically significant. The best-fit curves for the constant source density (0.0019 cm^{-3}) correspond to a source electron temperature of 1.3 keV for the active period, suggesting another possibility for this change.

The median value of the revised power is also largest in period (iii), followed in descending order by periods (i), (ii), and (iv). Auroral power is modulated by solar wind dynamic pressure (Kita et al., 2016). A linear relation between auroral power and solar wind was derived using the information at (ii) 0.037 and (iv) 0.021 nPa. For the pressure of 0.049 nPa of (iii), the total power derived from this linear relation is 1279 GW, which is slightly smaller than the observed power of 1355 GW, but the difference is not significant compared to the error averaged over the whole period, 281 GW.

The total energy emitted over 800 points (1 point = 10 min.) before ($10.4 < \text{DOY } 2015 < 52$), during ($45.8 < \text{DOY } 2015 < 82.5$), and after ($97.2 < \text{DOY } 2015 < 140$) the volcanic active period are 6.0×10^8 J, 7.6×10^8 J, and 6.4×10^8 J, respectively. Differences among the volcanic activity phases are much larger than 2.9×10^5 J, derived using the mean error. Additionally, the total energy input into the polar region during the entire event reaches 2×10^{19} J, which is comparable with the total energy content of the magnetospheric ions ~1.4×10^{19} J (Bagenal & Delamere, 2011).

4. Discussion

In the auroral feature, we found the following characteristic variations: (i) enhancements of the auroral power and its variation were caused by sporadic short-term (<1 rot to a few days) enhancements (Figure 1), and (ii) a relatively small color ratio, that is, auroral electron energy (Figures 2 and 3a–3c), observed during DOY 40–120 of 2015. It is known that volcanic eruptions (outbursts) last days, and the torus enhancement lasts from a few to tens of days. For this volcanic event in early 2015, the increase in infrared emission at Kurdalagon Patera was observed on DOY 26, sodium emission began on DOY 10 until its peak on ~DOY 50 (e.g., Yoneda et al., 2015), and OI emission began on DOY 20 and peaked during DOY 40–60 (Koga et al., 2018). Moreover, plasma transfer from the IPT (~6 R_J) to the middle magnetosphere of the main auroral source region (~20 R_J) is suggested to take tens of days (Bagenal & Delamere, 2011). Therefore, the variations observed during DOY 40–120 reflect an enhanced plasma transfer at the middle magnetosphere. There are other periods with smaller CR and sporadic enhancements at the beginning of season 2015, during DOY −40 to −10. This might have been affected by another volcanic event in late 2014, as reported by de Kleer and de Pater (2016); this was prior to the Hisaki and sodium monitors, and therefore beyond our data set. First, we qualitatively compare these parameters with the quiet period, followed by comparison with previous findings obtained using different methods.

Hisaki's long-term monitoring provides the following statistical auroral parameters: the total electron flux precipitation into the polar region of 54.2 ± 30 MA and appearance-revised total emission power of 1276 ± 810 GW. The total electron flux is comparable with the plasma corotation-enforcement current of 60–100 MA derived as a curl of the magnetic field measurement (Khurana, 2001). The revised total power is also comparable with other analyses, for example, 1.2 TW (Badman et al., 2016).

For the auroral enhancement event of season 2014, the enhancement of the source current density is comparable with the magnetospheric adiabatic variation due to solar wind compression (see section 5.4 of Paper II for detail). The other possible process, that is, the positional change toward an open–closed boundary, is less probable here, referring to observation of auroral deposition toward low latitudes during the interval of increased Io plasma mass loading reported by Bonfond et al. (2011) and theoretical suggestions (e.g., Nichols & Cowley, 2005).

We apply the same analysis to the 66 events in 2014–2015 seasons whose revised power at 136.5–144.8 nm exceeds 45 GW. We refer to the maximum value of solar wind dynamic pressure over 4 days (from 2 days before to 2 days after the events), and the minimum value of the pressure over 2 days before the maximum pressure. These time spans are set by taking into account the solar wind model uncertainty of shock arrival and possible time lag of magnetospheric response. Magnetopause location is derived from the solar wind pressure using an empirical model (Huddleston et al., 1998). We estimated the density increase due to the

magnetospheric compression assuming isotropic shrinking under the conservation of mass and corresponding plasma temperature variation for the adiabatic change to obtain variation of the source current $j_{//0}$. Then the field-aligned current density for the observed electron energy is derived referring to the Knight theory. We compare the estimated increase ratio of the field-aligned current, R_{model}, with that directly estimated from the auroral spectral observation, R_{obs}. Figure 4a shows the relationship between R_{model} and R_{obs}. Since this model is based on the solar wind pressure variation, we exclude the events which are independent of the solar wind pressure enhancement (maximum pressure $<$0.1 nPa, 13 events) shown by small marks. If the variation follows this model, the relationship should be $R_{model} = R_{obs}$. Eighty-one percent of all events are $R_{obs}/R_{model} < 2$. Some events which deviated from the relationship, that is, $R_{model}/R_{obs} \geq 2$, are more frequently seen for the volcanic activity case (seven red points) compared to the quiet case (two blue points). In addition, the R_{obs}/R_{model} values increase with the increasing R_{obs}. This deviation from $R_{obs} = R_{model}$ indicates the contribution of the other processes beyond the above model and assumptions, for example, nonadiabatic plasma acceleration such as magnetospheric reconnection and local heating, especially for the volcanic active period and large enhancement events.

As seen in Figure 3, during the active volcanic phase, the typical relationship between the auroral mean energy and the flux shifts in a number of ways, for example: (i) to the more magnetospheric populated case, that is, from 0.0019 to 0.0027 cm^{-3} or (ii) to a lower temperature of the source plasma, that is, from 2.5 keV to 1.3 keV, for the constant density case, or a combination of both. According to Nichols (2011), as an increase in the auroral electron flux is achieved in the case corresponding to increase in background density, we will discuss the plasma increase, above case (i). Note that this population is the suprathermal electron (~a few keV) which can reach the planetary atmosphere compared with the more abundant cold component (~tens of eV) in the magnetosphere. This indicates that the energetic suprathermal electrons are also increased by the volcanic activity, while the neutrals and ionized plasma enhanced at IPT would be mainly the cold component. In addition, the estimated auroral electron energy decreases for the active period, indicating a smaller acceleration. This behavior likely arises because the greater population of the source plasma would be enough to maintain the corotation enforcement current with less electron energy enhancement. A spectral diagnosis of the IPT emission observed by Hisaki suggests the enhancement of the cold (~several eV) and hot (~hundrds of eV) electron density during the period of Io-enhanced activity (Kagitani et al., 2017, MOP; Yoshikawa et al., 2017) and also indicates that the hot electron population increases with distance from Jupiter (Yoshioka et al., 2017). Although there is a difference in radial distances between the location of IPT (~6 R_J) and the magnetospheric source region of the main aurora (~20 R_J), the auroral analysis additionally suggests the enhancements of the suprathermal plasma in the middle magnetosphere. According to a modeling study by Nichols (2011), the enhancement of the total current seen in this observation also supports the increase of the magnetosphere plasma population with increased plasma mass loading at Io. The plasma angular velocity deviates from the corotation at smaller radius with more rapid variation during the increased plasma mass-loading period. This provides a larger magnetospheric current as well as a field-aligned current, which has been observed as an increase in auroral emission power (Nichols, 2011).

Using spatially resolved auroral spectra, Gérard et al. (2016) (and partly Gustin et al., 2004 and Paper I) showed that the relation between auroral electron energy/CR and electron energy flux varies according to which specific auroral feature is considered. The relationship derived from the polar-integrated Hisaki data set is the spatially averaged characteristic, as discussed in Paper I. In addition, the estimated electron energies in this study are mean values and we cannot specify the auroral electron spectral change in detail, that is, whether a decrease of electron energy over the whole energy range, or a relative decrease (increase) of high-energy (low-energy) electrons, or a combination of these types of changes. These are open questions beyond the scope of our data set and present analysis. We need to develop additional methods to ascertain whether other acceleration processes are dominant.

5. Summary

Long-term monitoring of Jupiter's aurora by Hisaki/EXCEED has detected enhancements of the auroral power with a strong sporadic response (by a factor of 2) and a decrease in the color ratio, that is, the auroral electron energy (by up to 30%), associated with reported Io volcanic events observed in early 2015. The enhanced plasma mass-loading of Io increases the source current via an increased suprathermal (a few keV) plasma

density by up to 42%, which contributes to a large field-aligned current to maintain the corotation with less field-aligned acceleration. Sporadic large auroral enhancements during the interval are not readily explained by an adiabatic solar wind response model, which suggests a contribution by nonadiabatic magnetospheric energization.

Acknowledgments
We acknowledge the working teams of Hisaki/EXCEED, WIND, ACE, and OMNI. The data from the Hisaki spacecraft can be found in the Data Archives and Transmission System (DARTS) of JAXA. The OMNI data used for the solar wind model were taken from the NASA Coordinated Data Analysis Web (CAWeb). This work was supported by MEXT/JSPS KAKENHI grants JP15K17769 and JP15H05209. SVB was supported by STFC Ernest Rutherford Fellowship ST/M005534/1. This work was carried out by the joint research program of the Institute for Space-Earth Environmental Research, Nagoya University. We acknowledge the contribution of the International Space Sciences Institute (ISSI) in Bern, Switzerland, for hosting and funding the ISSI international teams on "The influence of Io on Jupiter's magnetosphere" (ID388) and "How does the solar wind influence the giant planet magnetospheres?" (ID357) and the constructive discussions had by these team members. We thank NASA Hisaki PSP members for useful discussions. CT acknowledges to reviewers for constructive comments.

References

Badman, S. V., Bonfond, B., Fujimoto, M., Gray, R. L., Kasaba, Y., Kasahara, S., … Yoshioka, K. (2016). Weakening of Jupiter's main auroral emission during January 2014. *Geophysical Research Letters*, *43*, 988–997. https://doi.org/10.1002/2015GL067366

Bagenal, F., & Delamere, P. A. (2011). Flow of mass and energy in the magnetospheres of Jupiter and Saturn. *Journal of Geophysical Research*, *116*, A05209. https://doi.org/10.1029/2010JA016294

Bonfond, B., Vogt, M. F., Gérard, J.-C., Grodent, D., Radioti, A., & Coumans, V. (2011). Quasi-periodic polar flares at Jupiter: A signature of pulsed dayside reconnections? *Geophysical Research Letters*, *38*, L02104. https://doi.org/10.1029/2010GL045981

Connerney, J. E. P., Acuña, M. H., Ness, N. F., & Satoh, T. (1998). New models of Jupiter's magnetic field constrained by the Io flux tube footprint. *Journal of Geophysical Research*, *103*(A6), 11,929–11,939. https://doi.org/10.1029/97JA03726

Cowley, S. W. H., & Bunce, E. J. (2001). Origin of the main auroral oval in Jupiter's coupled magnetosphere-ionosphere system. *Planetary and Space Science*, *49*, 1067–1088.

de Kleer, K., & de Pater, I. (2016). Time variability of Io's volcanic activity from near-IR adaptive optics observations on 100 nights in 2013–2015. *Icarus*, *280*, 378–404.

Gérard, J.-C., Bonfond, B., Grodent, D., & Radioti, A. (2016). The color ratio-intensity relation in the Jovian aurora: Hubble observations of auroral components. *Planetary and Space Science*, *131*, 13–23.

Gustin, J., Gérard, J.-C., Grodent, D., Cowley, S. W. H., Clarke, J. T., & Grard, A. (2004). Energy-flux relationship in the FUV Jovian aurora deduced from HST-STIS spectral observations. *Journal of Geophysical Research*, *109*, A10205. https://doi.org/10.1029/2003JA010365

Hill, T. W. (1979). Inertial limit on corotation. *Journal of Geophysical Research*, *84*(A11), 6554–6558.

Hill, T. W. (2001). The Jovian auroral oval. *Journal of Geophysical Research*, *106*(A5), 8101–8107. https://doi.org/10.1029/2000JA000302

Huddleston, D. E., Russell, C. T., Kivelson, M. G., Khurana, K. K., & Bennett, L. (1998). The location of the Jovian bow shock and magnetopause: Galileo initial results. *Advances in Space Research*, *21*(11), 1463–1467.

Kagitani, M., Yoneda, M., Koga, R., Tsuchiya, F., Yoshioka, K., Murakami, G., … Yoshikawa, I. (2017). Variation of ion and electron temperature on Io plasma torus during an outburst measured with Hisaki/EXCEED and gourd-based telescope, Magnetospheres of the Outer Planets (MOP) conference abstract.

Khurana, K. K. (2001). Influence of solar wind on Jupiter's magnetosphere deduced from currents in the equatorial plane. *Journal of Geophysical Research*, *106*(A11), 25,999–26,016. https://doi.org/10.1029/2000JA000352

Kimura, T., Badman, S. V., Tao, C., Yoshioka, K., Murakami, G., Yamazaki, A., … Clarke, J. T. (2015). Transient internally driven aurora at Jupiter discovered by Hisaki and the Hubble Space Telescope. *Geophysical Research Letters*, *42*, 1662–1668. https://doi.org/10.1002/2015GL063272

Kita, H., Kimura, T., Tao, C., Tsuchiya, F., Misawa, H., Sakanoi, T., … Fujimoto, M. (2016). Characteristics of solar wind control on Jovian UV auroral activity deciphered by long-term Hisaki EXCEED observations: Evidence of preconditioning of the magnetosphere? *Geophysical Research Letters*, *43*, 6790–6798. https://doi.org/10.1002/2016GL069481

Koga, R., Tsuchiya, F., Kagitani, M., Sakanoi, T., Yoneda, M., Yoshioka, K., … Todd Smith, H. (2018). The time variation of atomic oxygen emission around Io during a volcanic event observed with Hisaki/EXCEED. *Icarus*, *299*, 300–307.

Nichols, J. D. (2011). Magnetosphere-ionosphere coupling in Jupiter's middle magnetosphere: Computations including a self-consistent current sheet magnetic field model. *Journal of Geophysical Research*, *116*, A10232. https://doi.org/10.1029/2011JA016922

Nichols, J. D., & Cowley, S. W. H. (2005). Magnetosphere-ionosphere coupling currents in Jupiter's middle magnetosphere: Effect of magnetosphere-ionosphere decoupling by field-aligned auroral voltages. *Annales de Geophysique*, *23*, 799–808.

Tao, C., Fujiwara, H., & Kasaba, Y. (2010). Jovian magnetosphere-ionosphere current system characterized by diurnal variation of ionospheric conductance. *Planetary and Space Science*, *58*, 351–364. https://doi.org/10.1016/j.pss.2009.10.005

Tao, C., Kataoka, R., Fukunishi, H., Takahashi, Y., & Yokoyama, T. (2005). Magnetic field variations in the Jovian magnetotail induced by solar wind dynamic pressure enhancements. *Journal of Geophysical Research*, *110*, A11208. https://doi.org/10.1029/2004JA010959

Tao, C., Kimura, T., Badman, S. V., André, N., Tsuchiya, F., Murakami, G., … Fujimoto, M. (2016). Variation of Jupiter's aurora observed by Hisaki/EXCEED: 2. Estimations of auroral parameters and magnetospheric dynamics. *Journal of Geophysical Research: Space Physics*, *121*, 4055–4071. https://doi.org/10.1002/2015JA021272

Tao, C., Kimura, T., Badman, S. V., Murakami, G., Yoshioka, K., Tsuchiya, F., … Fujimoto, M. (2016). Variation of Jupiter's aurora observed by Hisaki/EXCEED: 1. Observed characteristics of the auroral electron energies compared with observations performed using HST/STIS. *Journal of Geophysical Research: Space Physics*, *121*, 4041–4054. https://doi.org/10.1002/2015JA021271

Tsuchiya, F., Kimura, T., Yoshioka, K., Yoneda, M., Koga, R., Kagitani, M., … HISAKI science team> (2017). Enhancement of Jovian magnetospheric plasma circulation due to mass supply change from the satellite Io, Magnetospheres of the Outer Planets (MOP) abstract. Retrieved from https://www.irfu.se/mop2017/MOP2017_ProgrammeBook.pdf

Yamazaki, A., Tsuchiya, F., Sakanoi, T., Uemizu, K., Yoshioka, K., Murakami, G., … Sawai, S. (2014). Field-of-view guiding camera on the HISAKI (SPRINT-A) satellite. *Space Science Reviews*, *184*(1-4), 259–274. https://doi.org/10.1007/s11214-014-0106-y

Yoneda, M., Kagitani, M., & Okano, S. (2009). Short-term variation of Jupiter's extended sodium nebula. *Icarus*, *204*, 589–596.

Yoneda, M., Kagitani, M., Tsuchiya, F., Sakanoi, T., & Okano, S. (2015). Brightening event seen in observations of Jupiter's extended sodium nebula. *Icarus*, *261*, 31–33.

Yoneda, M., Tsuchiya, F., Misawa, H., Bonfond, B., Tao, C., Kagitani, M., & Okano, S. (2013). Io's volcanism controls Jupiter's radio emissions. *Geophysical Research Letters*, *40*, 671–675. https://doi.org/10.1002/grl.50095

Yoshikawa, I., Suzuki, F., Hikida, R., Yoshioka, K., Murakami, G., Tsuchiya, F., … Fujimoto, M. (2017). Volcanic activity on Io and its influence on the dynamics of the Jovian magnetosphere observed by EXCEED/Hisaki in 2015. *Earth, Planets and Space--Frontier Letter*, *69*(1), 110. https://doi.org/10.1186/s40623-017-0700-9

Yoshikawa, I., Yoshioka, K., Murakami, G., Yamazaki, A., Tsuchiya, F., Kagitani, M., … Tadokoro, H. (2014). Extreme ultraviolet radiation measurement for planetary atmospheres/magnetospheres from the earth-orbiting spacecraft (Extreme Ultraviolet Spectroscope for Exospheric Dynamics: EXCEED). *Space Science Reviews*, *184*(1-4), 237–258. https://doi.org/10.1007/s11214-014-0077-z

Yoshioka, K., Murakami, G., Yamazaki, A., Tsuchiya, F., Kagitani, M., Sakanoi, T., … Yoshikawa, I. (2013). The extreme ultraviolet spectroscope for planetary science, EXCEED. *Planetary and Space Science*, *85*, 250–260. https://doi.org/10.1016/j.pss.2013.06.021

Yoshioka, K., Tsuchiya, F., Kimura, T., Kagitani, M., Murakami, G., Yamazaki, A., … Fujimoto, M. (2017). Radial variation of sulfur and oxygen ions in the Io plasma torus as deduced from remote observations by Hisaki. *Journal of Geophysical Research: Space Physics*, *122*, 2999–3012. https://doi.org/10.1002/2016JA023691